RSC Advances

ROYAL SOCIETY OF CHEMISTRY

www.rsc.org/advances

Journal Name

RSCPublishing

ARTICLE

Synthesis of Carbon Xerogel Nanoparticles by Inverse Emulsion Polymerization of Resorcinol-Formaldehyde and Their Use as Anode Materials for Lithium-ion Battery

Cite this: DOI: 10.1039/x0xx00000x

Received 00th January 2012,
Accepted 00th January 2012

DOI: 10.1039/x0xx00000x

www.rsc.org/

Manohar Kakunuri, Sheetal Vennamalla and Chandra S. Sharma*

Department of Chemical Engineering, Indian Institute of Technology, Hyderabad, Yeddumailaram-502205, Telangana., India.

Abstract

Carbon xerogel nanoparticles were synthesized using repeated inverse emulsion polymerization of resorcinol-formaldehyde, followed by subcritical drying and pyrolysis at 1173 K. Thus prepared carbon xerogel nanoparticles were then structurally characterized by scanning electron microscopy, Raman spectroscopy, X-ray diffraction, transmission electron microscopy and small angle X-ray scattering. Further these carbon xerogel nanoparticles were tested for their electrochemical properties. Galvanostat charge/discharge experiments revealed their reversible capacity (400 mAh/g) higher than that of graphite with excellent capacity retention and coulombic efficiency. Cyclic voltammetry and impedance spectroscopic studies were also carried out to support these findings. The remarkable electrochemical behaviour as exhibited by these carbon xerogel nanoparticles paves the way for their potential use as anode materials in Lithium-ion battery.

Keywords: Carbon xerogel nanoparticles, Resorcinol-formaldehyde, Inverse emulsification, Reversible capacity, Anode materials, Lithium-ion battery.

***Corresponding Author**. Tel.: +91-40-2301-6112; Fax: +91-40-23016032; E-mail: cssharma@iith.ac.in

Introduction

Resorcinol-formaldehyde (RF) sol has been extensively used as an organic precursor to synthesize carbon aerogel, cryogel and xerogel microspheres respectively using inverse emulsion polymerization.[1-11] As carbon cryogel and aerogel microspheres possess large surface area, these have been well studied for their use as electrochemical double layer capacitors due to their enhanced double layer capacitance.[12-14] On the other hand, carbon xerogel microspheres as produced by subcritical drying did not receive considerable attention in literature till recently as these are largely nonporous and have less surface area. However there are few studies on generating the porosity in carbon xerogels either by activation or by tailoring the process conditions.[15-18] Recently, carbon xerogels with varying morphology like fractal-like structures and microspheres with nanofeatures have also been reported to expand their horizons for wider range of engineering applications due to their large external surface area.[10,11,19]

In this work, we report a facile way to synthesize interconnected carbon xerogel nanoparticles by repetitive inverse emulsion polymerization of RF gel followed by subcritical drying followed by pyrolysis in the nitrogen atmosphere. There are only few recent reports available in literature on synthesis of RF derived carbon nanospheres by electrospraying, surfactant templating and using chemical reagents.[20-23] Some of these techniques either lack in bulk production of carbon nanoparticles or are too complex and need very careful control. However the method presented in this work is facile and only needs to follow inverse emulsification process multiple times.

Further we have measured the electrochemical properties of these interconnected carbon xerogel nanoparticles to enable their use as anode materials for rechargeable lithium-ion battery. In commercial lithium-ion batteries, graphite is most commonly used anode material for which theoretical lithium-ion intercalation capacity is 372 mAh/g. However the lithium-ion intercalation capacity for RF derived carbon xerogel powder as reported previously was significantly less (145 mAh/g).[24] Even for three dimensionally ordered microporous interconnected RF derived carbon monolith as prepared by PMMA template showed reversible capacity nearly 195 mAh/g at similar current density (40 mA/g).[25] Further for RF derived carbon cryogel hollow particles reversible capacity was reported to be as high as 330 mAh/g.[26] To the best of our

knowledge, this is not only the first report on RF derived carbon xerogel nanoparticles as synthesized by inverse emulsion polymerization to be tested as anode materials for Lithium-ion battery but the reversible capacity as reported here is also higher than that of graphite. Our belief is that the excellent electrochemical behaviour of RF derived interconnected carbon xerogel nanoparticles as reported in this work may have a far reaching effect in providing an alternative to graphite as commercial Lithium-ion battery anode material.

Experimental section

Materials

Resorcinol (99% purity), formaldehyde (37% w/v; stabilized with about 10% methanol), potassium carbonate (98% purity), LP-30 electrolyte (1 M LiPF6 in 1:1 v/v mixture of ethylene carbonate and diethyl carbonate), non-ionic surfactant Span -80 (sorbitan monooleate, HLB value: 4.3) were purchased from Merck, India. Lithium foil (99.9% trace metal basis) was purchased from Sigma Aldrich, India while cyclohexane (99% purity) was purchased from Alfa Aeser, India. Stainless steel (SS) foil (polycrystalline SS 316, 100 µm thick) used as a substrate for cell testing was purchased from MTI corp., USA.

Preparation of RF sol

RF sol was prepared by polycondensation of resorcinol and formaldehyde, using deionized (DI) water as solvent. K_2CO_3 was added as catalyst to accelerate the polymerization reaction. The molar ratios of regents used were 1R: 2F: 27.03W: 0.04C. Resorcinol was dissolved in formaldehyde and stirred for 10 min to get clear solution. $K_2CO_3$was separately dissolved in DI water to form a clear solution. These two solutions were then mixed and stirred for about 30 min until golden yellow color RF sol was obtained.

Inverse emulsion polymerization

Thus obtained 0.5 ml of RF sol (water phase) was added drop wise to oil phase composed of 25 ml of cyclohexane solution and 12.5 ml of non-ionic surfactant span-80 (amphiphilic surface active agent), which minimizes interfacial tension at the boundary of two immiscible phases. In first cycle, inverse-emulsion system containing two immiscible phase was stirred with magnetic stirrer at 500 rpm for 5 h at room temperature to obtain RF particles followed by sedimentation for 12 h. Sedimentation allows settling of RF particles in a beaker and then allowing to replace supernate above the sediment with equal volume of fresh cyclohexane. This emulsion, with fresh cyclohexane was again stirred for 5 h at room temperature followed by 12 h sedimentation again. The lighter phase rich in cyclohexane was filtered and gravity settled RF particles after second cycle of inverse emulsification were then collected on SS foil used as a substrate followed by keeping them inside vacuum desiccator for 10 min to remove any traces of air bubbles. After degassing samples were dried in oven at 60 °C for 12 h to evaporate solvent yielding RF xerogel nanoparticles. A schematic explaining the above experimental steps to synthesize RF derived xerogel nanoparticles is shown as Fig. 1.

Pyrolysis

Dried RF xerogel nanoparticles samples were pyrolyzed in alumina tube furnace (Nabertherm GMBH). After introducing samples into furnace tube, tube was purged for 20 min with 1.5 l/min of N_2 flow. Once purged, N_2 flow rate was maintained at 0.5 l/min throughout the pyrolysis process. First temperature was raised to 900 °C with the ramp rate of 5 °C/min, then temperature was maintained at 900 °C for 1 h followed by cooling to room temperature in presence of N_2 flow.

Characterization

Field emission scanning electron microscope (FESEM, SUPRA 40, Zeiss) was used to observe the surface morphology of RF derived carbon xerogel nanoparticles. Structural characterization for as-synthesized carbon xerogel nanoparticles was carried out using PANalytical X-ray diffractometer with CuKα radiation and Raman spectroscopy recorded with a 532 nm laser on Bruker Raman microscope (Model: Senterra). Point collimation small angle x-ray scattering (SAXS) (SAXess, Anton-Paar) system with CuKα radiation (0.154 nm) was used to record scattering between 0.01 to 10 nm^{-1} q-range under vacuum at room temperature to estimate radius of gyration and surface area. Carbon xerogel powder was placed between two copper plates with the help of X-ray transparent krypton film. However scattering data for background and sample was collected using image plate for 30 min, and background subtracted scattering file was used for further analysis. High resolution micrographs were recorded with transmission electron microscopy (HRTEM, FEI Tecnai G2S-Twin) operated at 200 kV.

For electrochemical studies, the SS foil with carbon xerogel nanoparticles deposited on it was used as a working electrode and lithium metal as a reference electrode (counter electrode). Glass microfiber filters (Whatman, Grade GF/D) was used as separator while 1 M LiPF6 in 1:1 v/v mixture of ethylene carbonate and diethyl carbonate (LP-30) was used as electrolyte. All these components of lithium-ion battery testing set up were tightly packed inside argon filled glove box using Swagelok cell assembly and soaked for 12 h before electrochemical testing. Electrochemical characteristics for packed half-cell were investigated using Potentiostat/Galvanostat (Bio-Logic Science Instruments, Model VSP).

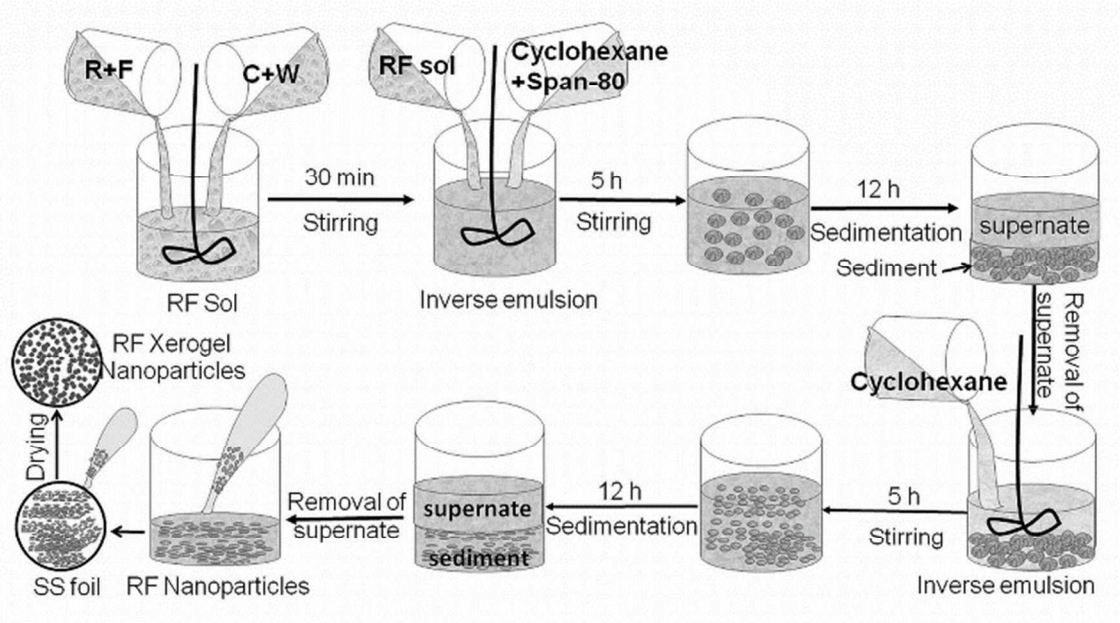

Figure 1: Schematic showing the various steps of synthesis of RF xerogel nanoparticles using repetitive inverse emulsion polymerization

Results and discussion

Surface Morphology

Fig. 2 shows the FESEM images of interconnected carbon xerogel nanoparticles prepared by pyrolyzing RF xerogel particles at 900 °C collected from the sediments after first and second cycles of inverse emulsification. After first cycle of stirring followed by gravity sedimentation, we observed large aggregates of RF particles (Fig. 2a-b). This may be due to coalescence between individual RF sol particles. However during second cycle of inverse emulsification, gelation of RF sol droplets might be complete which prevents further coalescence. Continuous stirring may though allow further breakage of individual RF gel droplets into nano-sized particles (Fig. 2c-d).

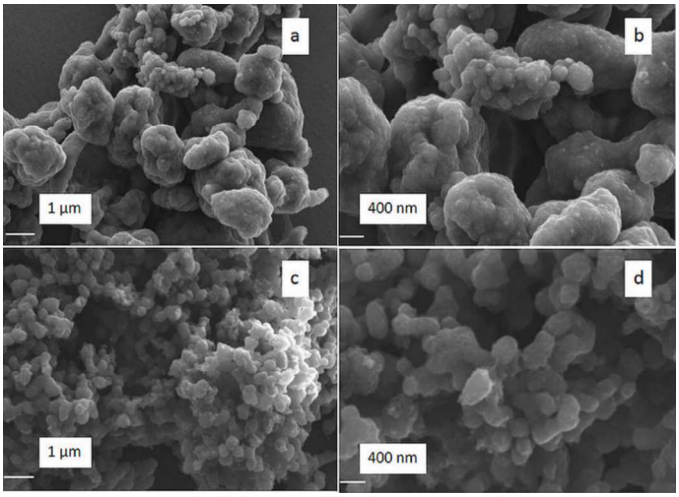

Figure 2: Low and high magnification FESEM images of carbon xerogel nanoparticles network (a-b) sample collected from sediment after 12 h sedimentation of first cycle; (c-d) sample collected after 12 h sedimentation of second cycle.

Samples were collected from the sediments to deposit high density of RF xerogel particles on substrate. This uniform and sufficiently dense layer deposition of RF xerogel nanoparticles was required to prepare the continuous interconnected network of carbon xerogel nanoparticles upon pyrolysis which were further tested for electrochemical testing.

Structural characterization

Fig. 3 shows the Raman spectra for as-synthesized RF derived carbon xerogel nanoparticles. Broad peaks as associated with characteristic D and G band of carbon may be attributed to small crystallite thickness of amorphous carbon.[27] G band at 1592 cm^{-1} corresponds to the in-plane vibrations of carbon atoms strongly coupled in graphene sheet. Broad D band at 1331 cm^{-1} attributed to dangling bonds and defects of prepared carbon structure. Intensity ratio of D peak and G peak (ID/IG) was calculated to be 1.01, and correspondingly in-plane crystallite thickness was calculated as 4.23 nm (La=4.4 / (ID/IG)).[28]

XRD pattern of RF derived carbon xerogel nanoparticles is shown in Fig. 4. Two broad peaks at 2θ=24° and 43.8° corresponds to (0 0 2) and (1 0 0) reflections respectively.[28] Broad peak at 2θ=24° confirms the amorphous nature of carbon. Mean stack height of crystallite was calculated as 10 A° by applying Scherrer's formula to (0 0 2) diffraction peak. Interlayer spacing (d_{002}) was measured to be 3.71 A° using Bragg's law.

HRTEM images as shown in Fig. 5 reveals the agglomerated carbon xerogel particles. At high magnification, randomly positioned short range graphitic crystallites were observed with amorphous nature of carbon. Interlayer spacing in these crystallites was measured to be 3.55 A° through TEM image. These observations are consistent with the XRD and Raman analysis.

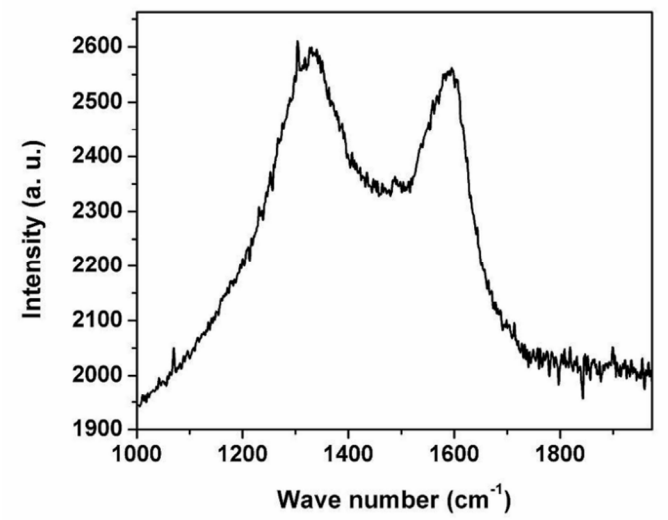

Figure 3: Raman spectrum of RF derived carbon xerogel nanoparticles.

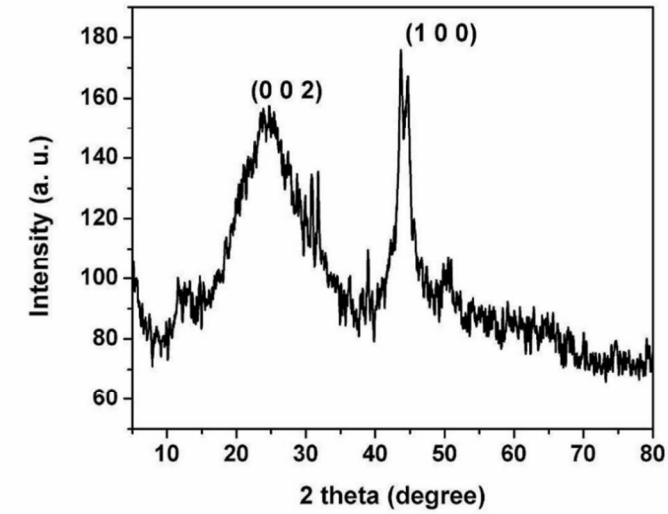

Figure 4: XRD spectrum of RF derived carbon xerogel nanoparticles.

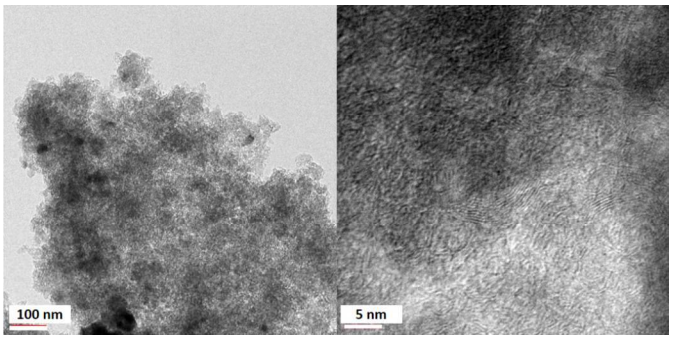

Figure 5. TEM images of samples carbon xerogel nanoparticels

SAXS analysis

Small angle x-ray scattering curve of carbon xerogel nanoparticles is shown as Fig. 6, where q is scattering vector that depends on diffraction angle (2θ) and source wavelength (λ). Radius of gyration R_g as defined by root-mean-square distance from the centre of gravity to electrons in scattering entity can be calculated by Guinier plot (I (q) versus q^2) as shown in the inset image of Fig. 6 using the equation [1].[29,30]

$$logI(q) = logI_0 - (\frac{R_g^2}{3}.q^2) \quad [1]$$

Radius of gyration was calculated to be 2.46 nm for the RF derived carbon xerogel nanoparticles. Surface to volume ratio was calculated as 823 m^2/cm^3 from Porod analysis using SAXSquant software. Specific surface area was then calculated to be 685.8 m^2/g by dividing surface to volume ratio with density of carbon xerogel (1.2 g/cm^3). [18]

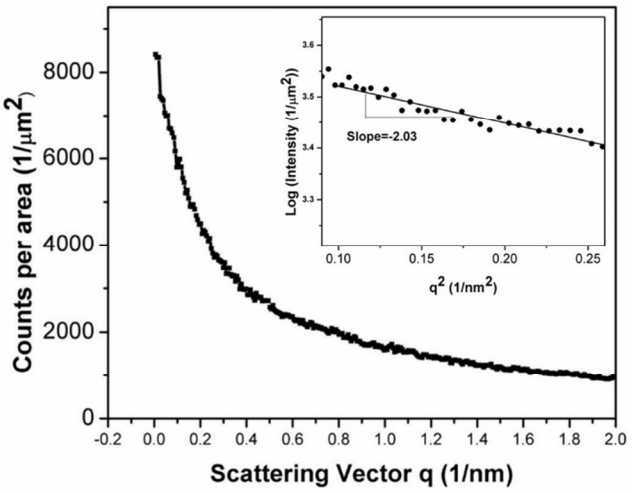

Figure 6. Small angle X-ray scattering curve for RF derived carbon xerogel nanoparticles

Electrochemical Performance

Cyclic voltammetry

Fig. 7 shows the cyclic voltammogram for RF derived carbon xerogel nanoparticles recorded with 0.1 mV/s of scan rate in the voltage range of 0-3 V. Cathodic current broad peak between 0.5 V and 1 V of first two cycles corresponds to formation of so called insoluble and electronically insulating solid electrolyte interface due to decomposition of electrolyte to form lithium oxides, carbonates and halides. Another sharp peak near 0 V (<0.25 V) corresponds to reversible insertion of lithium into carbon xerogel nanoparticles.[31, 32] Anodic peak in all four cycles about 1.2 V corresponds to de-insertion of lithium ions from the carbon xerogel particles.

Galvanostatic charge-discharge experiments

Galvanostatic charge discharge cycling experiments were carried out at room temperature, between 0.01 V and 3 V at current density of 37.2 mA/g (0.1 C). Fig.8 shows the charge/discharge profiles for RF derived carbon xerogel nanoparticles for 100 cycles. As clearly observed first discharge capacity was very large (1127 mAh/g) compared to subsequent cycles due to electrolyte decomposition to form SEI layer as also observed a plateau at 0.8 V.[32] This plateau is replaced with sloping curve in further cycles due to heterogeneous lithium-ion insertion mechanism.[33] This observation is also supported by cyclovoltammogram (Fig. 7) where there is a peak at 0.8 V corresponding to SEI layer formation in carbon materials. The large specific surface area as measured by SAXS analysis is also potential source for this SEI layer formation. Fig. 9 summarizes the cycling performance of RF derived carbon xerogel nanoparticles for 100 cycles. After 30 cycles of

charge/discharge, the reversible capacity was stabilized at ~400 mAh/g, even larger than that of graphite. Coulombic efficiency as defined by the ratio of discharge to charge capacity was also found to be more than 95% after initial five cycles. Initial coulombic efficiency is about 44%, for due credit to SEI layer formation.

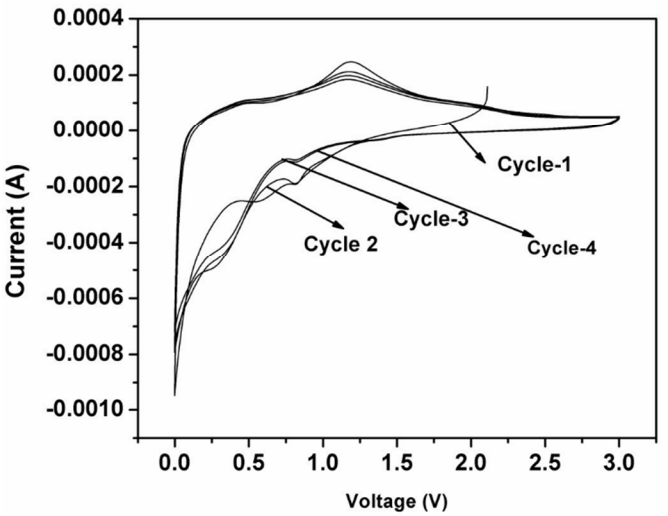

Figure 7: Cyclic voltammogram of carbon xerogel nanoparticles at scan rate of 0.1 mV/s.

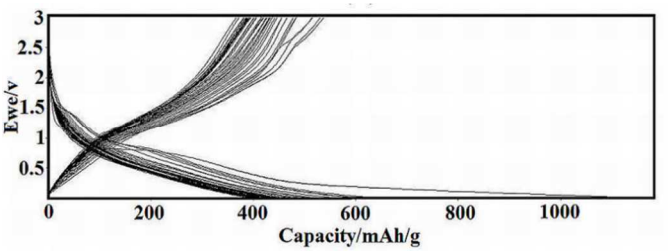

Figure 8: Charge-discharge profiles of RF derived carbon xerogel nanoparticles at 0.1 C rate in the voltage range of 0.01-3.0 V.

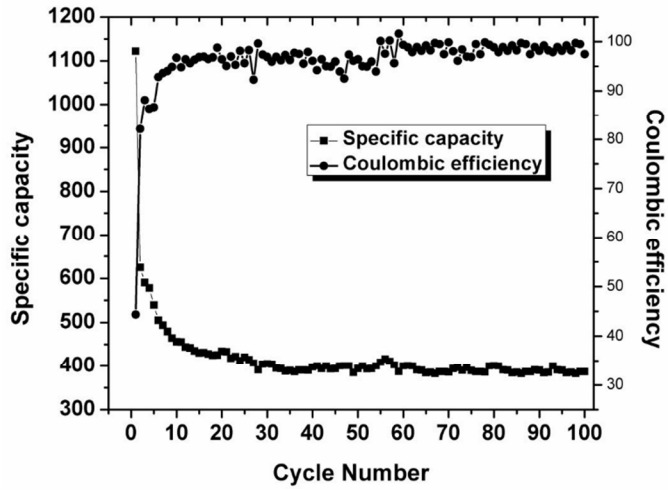

Figure 9: Cycling performance of carbon xerogel nanoparticles.

Further we provided a quick summary of electrochemical performance of various other organic gel materials as reportedly used in literature as anode (Table 1).[24-26, 34, 36-38] It can be clearly observed that RF xerogel derived carbon nanoparticles not only exhibited higher coulombic efficiency in first cycle but also showed higher specific reversible capacity even after 100 cycles. Also, initial reversible capacity for RF xerogel derived carbon nanoparticles was significantly higher than RF based aerogel and cryogels.[26,36] Our results in this work are only comparable to what has been reported for carbon nanospheres prepared by carbonizing polypyrrole nanospheres.[34] However in that case also, cyclic behaviour is reported up to 60 charge/discharge cycles in contrast of 100 cycles reported in the present work. These results clearly indicate the superior electrochemical behaviour of as-prepared RF derived carbon xerogel nanoparticles even as compared to graphite which is most widely used anode material in commercial Li ion battery.[35]

This exceptional cyclic performance for RF derived carbon xerogel nanoparticles may be attributed to facile diffusion between interconnected particles due to smaller diffusion length (radius of gyration 2.46 nm) and adsorption of lithium on the nanopores formed by small crystallites arrangement like house of cards with small in-plane crystallite thickness and mean stack height of crystallite as shown by XRD and Raman spectra.[39] The better performance of carbon xerogel nanoparticles can also be attributed to composite structure of crystallites and amorphous carbon like hard carbon as shown in Fig. 5, where hard carbons allow more lithium insertion and graphitic crystallites improves the electronic conductivity.[40]

Electrochemical Impedance Spectroscopy

EIS measurements were also carried out before cycling and after 10 cycles of charge discharge and results are summarized in Fig. 10 a-b respectively. Nyquist plot was obtained with 10 mV perturbation over the range of 10 mHz -100 kHz. Fig. 10 a-b shows out of shaped semi circles in high frequency range and an inclined straight line in low frequency range. As observed in Fig. 10a, charge transfer resistance for RF derived carbon xerogel nanoparticles was very less (8.9 Ω) that further suggests better electrical conductivity between particles network and efficient contact between current collector and carbon xerogel particles. After cycling, increase in charge transfer resistance to 69.5 Ω may be attributed to SEI layer formation and collapse of structure during insertion and extraction of Li ions. These findings are in line with structural characteristics of RF derived carbon xerogel nanoparticles such as large specific surface area, smaller R_g and crystalline arrangement like house of cards, as discussed above.

Journal Name

RSCPublishing

ARTICLE

Table 1. Summary of electrochemical performance of previously reported carbon gel materials and a comparison with present work

Sample Type	1st cycle reversible capacity (mAh/g) / coulombic efficiency (%)	Number of cycles reported (n)	Specific Capacity after 'n' cycles (mAh/g) / Current density
Carbon xerogel (powder)[24]	171 / 43	30	145 / 100 mA/g
Three dimensional ordered microporous carbon[25]	223 / 42	30	195/ 40 mA/g
	300 / 43	01	300 / 15.2 mA/g
Carbon cryogel hollow microspheres[26]	164 / 33	5	155 / 0.15 mA/cm^2
Carbon cryogel microcapsules[26]	360 / 34	5	340 / 0.15 mA/cm^2
Carbon cryogel microspheres[26]	140 / 32	5	130 / 0.15 mA/cm^2
Pyrrole derived carbon nanospheres[34]	423 / 72	60	420 / 60 mA/g
Carbon aerogel[36]	312 / 20	50	242 / 50 mA/g
Phenol-melamine-formaldehyde- resin (PMFR) derived carbon[37]	194 / 38.8	20	184 / 100 mA/g
Nitrogen doped porous carbon xerogel[38]	275/ 43	50	212 / 37.2 mA/g
Carbon Xerogel nanoparticles (Present work)	**497 / 44**	**100**	**385/ 37.2 mA/g**

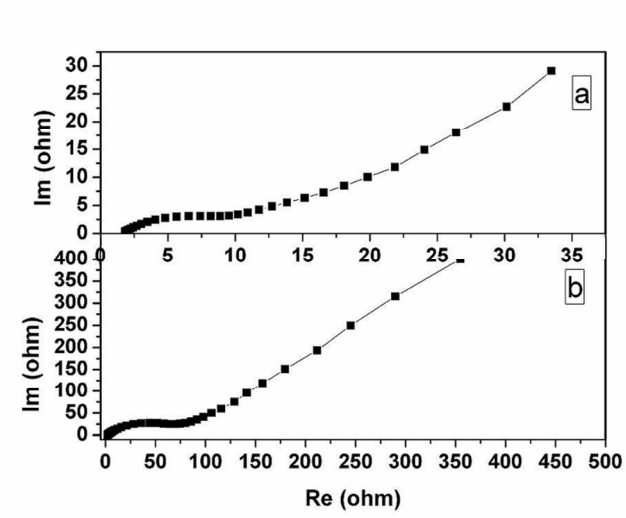

Figure 10: Electrochemical impedance spectra of RF derived carbon xerogel nanoparticles (a) at open circuit voltage, (b) after 10 cycles.

Conclusions

Carbon xerogel nanoparticles have been synthesized using sedimentation assisted inverse emulsion polymerization of resorcinol and formaldehyde followed by drying in air before pyrolysis at 900 °C. XRD, TEM and Raman analysis confirmed the amorphous nature with small crystallites arrangement. Galvanostat charge-discharge experiments showed the reversible capacity even higher than that of graphite and other carbon xerogel, aerogel and cryogel derived carbon with improved cyclability and capacity retention while minimizing the irreversible capacity losses. Electrochemical impedance spectra studies also supplemented these findings with very minimal charge transfer resistance due to reduced diffusion length. High irreversible capacity of initial cycle may be attributed to large specific surface area of carbon xerogel nanoparticles as calculated from SAXS analysis. In summary, the excellent cyclic performance with higher coulombic efficiency and capacity retention for RF derived carbon xerogel nanoparticles make them potential alternatives as anode materials for Lithium-ion battery. Further this study may add new perspectives in the study of carbon xerogels for their use in energy storage devices, in general.

Acknowledgments

SV acknowledges Surya Raj for his initial help with experiments. CSS acknowledges the Indian Institute of Technology, Hyderabad for providing necessary research infrastructure to carry out this work.

References

1 C. T. Alviso, R. W. Pekala, J. Gross, X. Lu, R. Caps, J. Fricke, *Materials Research Society Symposium Proceedings*, 1996, **431,** 521.
2 X. Wang, X. Wang, L. Liu, L. Bai, H. An, L. Zheng, Y. Lanhua, *Journal of Non-Crystalline Solids*, 2011, **357**, 793.
3 T. Horikawa, J. Hayashi, K. Muroyama, *Carbon*, 2004, **42**, 169-175.
4 A. Soottitantawat, T. Yamamoto, A. Endo, T. Ohmori, M. Nakaiwa, *AIChE Journal,* 2007, **53**, 228.
5 S. Kim, T. Yamamoto, A. Endo, T. Ohmori, M. Nakaiwa, *Journal of Industrial and Engineering Chemistry*, 2006, **12**: 484.
6 T. Yamamoto, A. Endo, T. Ohmori, M. Nakaiwa, *Carbon*, 2005, **43,** 1231.
7 H. Zhang, F. Ye, H. Xu, L. Liu, H. Guo, *Materials Letters*, 2010, **64**, 1473.
8 S. A. Al-Muhtaseb, J. A. Ritter, *Advanced Materials*, 2003, **15**, 101.
9 T. Yamamoto, A. Endo, T. Ohmori, M. Nakaiwa, *Carbon,* 2004, **42**, 1671.
10 C. S. Sharma, M. M. Kulkarni, A. Sharma, M. Madou, *Chemical Engineering Science*, 2009, **64**, 1536.
11 C. S. Sharma, D. K. Upadhyay, A. Sharma, *Industrial & Engineering Chemistry Research*, 2009, **48,** 8030.
12 B. Babic, B. Kaluderovic, L. Vracar, N. Krstajic, *Carbon*, 2004, **42,** 2617.
13 J. Li, X. Wang, Q. Huang, S. Gamboa, P. J. Sebastian, *Journal of Power Sources*, 2006, **158**, 784.
14 R. W. Pekala, J. C. Farmer, C.T. Alviso, T. D. Tran, S. T. Mayer, J. M. Miller, B. Dunn, *Journal of Non-Crystalline Solids,* 1998, **225,** 74.
15 C. Lin, J. A. Ritter, *Carbon* 2000, **38**, 849.
16 I. Matos, S. Fernandes, L. Guerreiro, S. Barata, A. M. Ramos, J. Vital, I. M. Fonseca, *Microporous and Mesoporous Materials*, 2006, **92**, 38.
17 T. Tsuchiya, T. Mori, S. Iwamura, I. Ogino, S. R. Mukai, *Carbon*, 2014, **76**, 240.
18 S. Mezzavilla, C. Zanella, P. R. Aravind, C. D. Volpe, G. D. Soraru, *Journal of Materials Science*, 2012, **47**, 7175.
19 A. Awadallah-F, S. A. Al-Muhtaseb, *Materials Letters*, 2012, **87**, 31.
20 C. S. Sharma, S. Patil, S. Saurabh, A. Sharma, R. Venkataraghavan, *Bulletin of Material Science*, 2009, **32**, 239.
21 D. Tashima, E. Yamamoto, N. Kai, D. Fujikawa, G. Sakai, M. Otsubo, T. Kijima, *Carbon*, 2011, **49**, 4848.
22 Y. R. Dong, N. Nishiyama, Y. Egashira, K. Ueyama. *Industrial & Engineering Chemistry Research*, 2008, **47,** 4712.
23 D. Tashima, M. Taniguchi, D. Fujikawa, T. Kijima, M. Otsubo, *Materials Chemistry and Physics*, 2009, **115**, 69.
24 Y. Yuan, Y. J. Chao, Z. F. Ma, X. Deng, *Electrochemistry Communications*, 2007, **9**, 2591.
25 K. T. Lee, J. C. Lytle, N. S. Ergang, S. M. Oh, A. Stein, *Advanced Functional Materials*, 2005, **15**, 547.
26 H. Zhang, H. Xu, C. Zhao, *Materials chemistry and physics,* 2012, **113**, 42.
27 T. Jawhari, A. Roid, J. Casado, *Carbon*, 1995, **33**, 1561.
28 F. J. Maldonado-Hodar, C. Moreno-Castilla, J. Rivera-Utrilla, Y. Hanzawa, Y. Yamada, *Langmuir*, 2000, **16,** 4367.
29 G. Porod, in Small Angle X-ray Scattering, ed. O. Glatter and O. Kratky, Academic Press, New York, 1982, ch. 2, pp. 18.
30 H. Tamon, H. Ishizaka, *Journal of Colloid and Interface Science*, 1998, **206**, 577.
31 F. Galobardes, C. Wang, M. Madou, *Diamond and Related Materials*, 2006, **15**, 1930.
32 S. Zhang, M. S. Ding, K. Xu, J. Allen, T. R. Jow. *Electrochemical and Solid-State Letters*, 2011, **4**, A206.
33 W. Ai, L. Xie, Z. Du, Z. Zeng, J. Liu, H. Zhang, et al. *Scientific Reports*, 2013, **3**, 2314.
34 Y. Wang, F. Su, C. D. Wood, J. Y. Lee, X. S. Zhao, *Industrial & Engineering Chemistry Research*, 2008, **47**, 2294.
35 P. Ridgway, H. Zheng, A. F. Bello, X. Song, S. Xun, J. Chong, V. Battaglia, Journal of Electrochemical Society, 2012, **159(5)**, A520.
36 L. Nian-Ping, S. Jun, G. Da-Yong, L. Dong, Z. Xiao-Wei, L. Ya-Jie, *Acta Physico -Chimica Sinica*, 2013, **29 (5)**, 966.
37 Y. Zhu, X. Xiang, E. Liu, Y. Wu, H. Xie, Z. Wu, Y. Tian, *Materials Research Bulletin*, 2012, **47**, 2045.
38 X. Liu, S. Li, J. Mei, W. Lau, R. Mi, Y. Li, H. Liu, L. *Liu, Journal of materials chemistry A*, 2014**, 2**, 14429.
39 Y. Liu, J. S. Xue, T. Zheng, J. R. Dahn, *Carbon,* 1996, **34**, 193.
40 K. Kim, T. Lee, H. Kim, S. Lim, S. Lee, *ElectrochemicaActa*, 2014, **135,** 27

Table of Contents Graphic

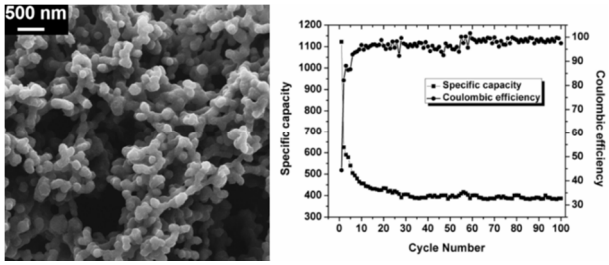

Resorcinol-formaldehyde (RF) derived carbon xerogel nanoparticles were synthesized using sedimentation assisted inverse emulsification process followed by simple oven drying and pyrolysis. These carbon xerogel nanoparticles based on the excellent electrochemical characteristics exhibited, find potential use as high capacity anode materials for Li ion battery.